Applications in Energy and Combustion Science 27 (2026) 100532

Contents lists available at ScienceDirect

Applications in Energy and Combustion Science

journal homepage: www.elsevier.com/locate/jaecs

Large eddy simulations of ventilation-limited compartment fire scenarios using a new dynamic flame extinction and re-ignition model in FDS☆

Georgios Maragkos [a],*, Jason Floyd [b], Andrea Lucherini [c], Alexander Snegirev [a], Elijah Igweh [a,c], Bart Merci [a]

[a] Department of Structural Engineering and Building Materials, Ghent University, Belgium
[b] Fire Safety Research Institute, UL Research Institutes, USA
[c] Department for Research of Fire-Safe Sustainable Environment (FRISSBE), Slovenian National Building and Civil Engineering Institute (ZAG), Slovenia

ARTICLE INFO

Keywords:
Flame extinction
Flame re-ignition
Compartment fire
Under-ventilated conditions
CFD modelling
FDS

ABSTRACT

Large eddy simulations of ventilation-controlled compartment fire scenarios conducted with FDS and new dynamic extinction and re-ignition models are presented. Flame extinction is modelled considering an enthalpy balance, based on a critical flame temperature, while re-ignition is allowed if the local resolved temperature exceeds a given re-ignition temperature. The re-ignition temperatures are estimated on the basis of counterflow simulations with hot oxidizers at different strain rates. The determination of the critical flame temperatures is made through well-stirred reactor simulations under different residence times and diluent types/concentrations. The new models are applied in reduced-scale ventilation-limited compartment fire scenarios with variable heat release rate. Comparison against the original model of FDS, relying on constant critical flame and re-ignition temperatures, are made. Overall, the predictions with the new dynamic models agree both qualitatively and quantitatively with the experiments. By considering the local properties of the flow, the new models bring some improvements, compared to the original models of FDS, in particular for the O_2 concentrations inside the compartment in ventilation-controlled conditions.

1. Introduction

Due to their significance in fire safety science and engineering, the study of compartment fires received a lot of attention in the past, e.g., [1–3]. With the increasing use of Computational Fluid Dynamics (CFD) as a tool to study fire dynamics in the built environment, there is also a plethora of CFD studies on this topic. These works range from reviewing the challenges and the different modelling approaches of such scenarios (e.g., [4–6]), performing rigorous CFD model validation (e.g., [7–10]), applying CFD models for simulating enclosure fire scenarios under various ventilation conditions (e.g., [11–16]) and analysing various specific fire dynamics aspects involved in enclosure fires (e.g. [17,18]).

In general, compartment fires are classified into two distinct regimes, namely ventilation-controlled (regime I) or fuel-controlled (regime II) scenarios [3]. In scenarios involving well-ventilated conditions no external flaming is expected since there is sufficient oxygen inside the compartment for the gaseous fuel to react. That is the case in scenarios when the fire is relatively small compared to the compartment (i.e., localized) and the fire is not located close to the ventilation opening(s). On the contrary, in scenarios involving under-ventilated conditions (e.g., as the Heat Release Rate (HRR) of the fire increases), external flaming can be observed as the fire tries to find sufficient oxygen for combustion.

However, simulations of such ventilation-controlled compartment fires with the Fire Dynamics Simulator (FDS) [19] still remain challenging. This may be attributed to possible limitations of the employed extinction and re-ignition sub-models (e.g., relying on constant critical flame and re-ignition temperatures, respectively), and the mesh dependence thereof. Some recent modelling efforts [15,20,21] involving the application of FDS in compartment scenarios involving flame extinction, have suggested that improvements in the re-ignition and extinction sub-models of FDS might be required for improving its accuracy when simulating such scenarios. The present study builds upon the knowledge gained from previous CFD studies and aims to enhance the current capabilities of FDS towards predicting flame extinction and re-ignition in under-ventilated compartment fire scenarios.

The main objective of this work is to apply the newly developed extinction model, previously presented in [22], to a series of ventilation-controlled compartment fire scenarios. It is worth noting that the

☆ This article is part of a Special issue entitled: 'Fires in Infrastructures' published in Applications in Energy and Combustion Science.

* Corresponding author.
E-mail address: georgios.maragkos@ugent.be (G. Maragkos).

https://doi.org/10.1016/j.jaecs.2026.100532
Received 30 April 2026; Received in revised form 5 June 2026; Accepted 21 June 2026
Available online 27 June 2026

development and validation of the model in two well-characterized open flame scenarios (i.e., UMD line burner and FM burner) was presented in [22], whereas the present work extends the model validation to compartment scenarios, of more practical significance to fire safety engineering. As such, the objective is to evaluate its performance and predictive capabilities towards accurately predicting flame extinction/re-ignition as well as the heat release rate inside and outside compartments. Emphasis is put on using the default FDS models and settings, typically used by fire safety engineers when performing numerical simulations of similar compartment fire scenarios. Comparisons are also made with the default extinction model of FDS in Large Eddy Simulation (LES) mode in order to evaluate whether the newly developed extinction model brings improvements in the CFD predictions.

2. Modelling

FDS version 6.9.1 [19] in LES mode has been used for the numerical simulations in the present study. FDS, developed by NIST, is a low-Mach number, second order accurate, finite difference code with explicit time integration. The default FDS models for turbulence, combustion and radiation have been used in the simulations presented here. This choice is intentional as these are the models that will be used by fire safety engineers when applying FDS to simulate various compartment fire scenarios. The novelty of the present work, in terms of modelling, is presented in Section 2.6 and it involves the dynamic calculation of the re-ignition and critical flame temperatures used by FDS when modelling flame re-ignition and extinction, respectively. This is an extension of the original approach used by FDS which considers constant values for both quantities for every fuel. More details regarding the available modelling options of FDS can be found in [23,24].

2.1. Turbulence modelling

Turbulence is modelled using a modified Deardorff model [25] calculating the sub-grid scale viscosity, μ_{sgs}, as:

$$\mu_{sgs} = \overline{\rho} C_v \Delta \sqrt{k_{sgs}} \tag{1}$$

where $C_v = 0.1$ [26] is a model constant.

The sub-grid scale kinetic energy, k_{sgs}, is calculated from an algebraic relationship, based on scale similarity, as:

$$k_{sgs} = \frac{1}{2}((\overline{u} - \hat{\overline{u}})^2 + (\overline{v} - \hat{\overline{v}})^2 + (\overline{w} - \hat{\overline{w}})^2) \tag{2}$$

where $\overline{u}$ is the LES filtered velocity at length scale Δ and $\hat{\overline{u}}$ is a weighted average of u over the adjacent cells. The terms $\overline{v}$, $\hat{\overline{v}}$, $\overline{w}$, $\hat{\overline{w}}$ are defined similarly [24].

2.2. Combustion modelling

The combustion model is mixing-controlled and considers a one-step, irreversible chemical reaction combined with the Eddy Dissipation Concept (EDC) [27] for modelling turbulence-chemistry interactions. As such, the fuel reaction rate, $\overline{\dot{\omega}'''_F}$, is calculated as:

$$\overline{\dot{\omega}'''_F} = -\overline{\rho} \frac{\min(\widetilde{Y}_F, \widetilde{Y}_{O_2}/s)}{\tau_{mix}} \tag{3}$$

where $\widetilde{Y}_F$ and $\widetilde{Y}_{O_2}$ are the fuel and oxygen mass fractions, respectively, and s is the stoichiometric oxygen-to-fuel mass ratio.

The mixing time scale, τ_{mix}, is calculated by comparing the mixing times for diffusion (i.e., τ_d), sub-grid scale advection (i.e., τ_u), and buoyant acceleration (i.e., τ_g) as [28]:

$$\tau_{mix} = \max(\tau_{chem}, \min(\tau_d, \tau_u, \tau_g, \tau_{flame})) \tag{4}$$

with

$$\tau_d = \frac{\Delta^2}{D_F}, \qquad \tau_u = \frac{C_u \Delta}{\sqrt{(2/3)k_{sgs}}}, \qquad \tau_g = \sqrt{\frac{2\Delta}{g}} \tag{5}$$

where D_F is the effective diffusivity of the fuel, and $C_u = 0.4$ [29] is a model constant calibrated to match Heskestad's flame height correlation [30]. The mixing time scale, τ_{mix}, is also bounded between a low (i.e., τ_{chem}) and an upper value (i.e., τ_{flame}).

2.3. Radiation modelling

Radiation is modelled considering that the radiation intensity is a function of spatial location and angular direction and is obtained by solving the radiative transfer equation, for a non-scattering medium, based on the finite volume method.

A gray gas model is employed in which the mixture absorption coefficient, κ, is calculated as the sum of the individual gases' gray coefficients, κ_i, for each specie i as:

$$\kappa = \sum_i \kappa_i(\widetilde{Y}_i, \widetilde{T}) \tag{6}$$

The gases' absorption coefficients, $\kappa_{n,i}$ are calculated by a narrow-band model, RADCAL [31], considering the minimum of a Planck mean coefficient (which depends on the local species composition and temperature) and an effective absorption coefficient (which depends on the local species composition, temperature and path length L) as:

$$\kappa_i = \min(\kappa_{i,P}, \kappa_{i,e}) \tag{7}$$

The default value for the path length in FDS is $L = 0.1$ m. For more details regarding radiation modelling in FDS the reader is referred to [24].

It is worth noting that radiation modelling is challenging in compartment fire scenarios, especially in limited ventilation conditions, since higher soot volume fractions are often met than in open fires. The fuel used in the experiments here (i.e., CH_4) is generally only weakly sooty and the experimental data in [32] also indicated that minimal soot concentrations were produced during the tests. As such, the effect of soot was not explicitly considered when calculating the absorption coefficients. Nevertheless, its potential influence is implicitly accounted for through the prescribed radiative fraction and the employed correction in the radiative emission.

In regions where reactions occur (i.e., $\chi_R \overline{\dot{q}'''} > 1$ kW/m^3), the radiative emission source term can be under-predicted if coarse grids are used in the simulations. As such, a correction term, C, is applied which is expressed as:

$$C = \frac{\sum(\chi_r \overline{\dot{q}'''} + \kappa G)V}{\sum(4\kappa\sigma\widetilde{T}^4)V} \tag{8}$$

where $\overline{\dot{q}'''}$, is the heat release rate per unit volume, χ_r is the radiative fraction of the fuel and V is the cell volume. Note that the correction, through the use of χ_r, defines the minimum amount of radiation that will be released from the fire. Also, the correction term is bounded between 0.1 and 100 to prevent spurious behaviour at the start of a simulation. Note that there is currently no Turbulence-Radiation Interaction (TRI) model available in FDS. However, the required correction in the radiative emission on coarse(r) grids is achieved through the correction term.

Finally, the radiative heat loss term in the energy equation is estimated as:

$$\nabla \cdot \overline{q''_r} = \kappa(4\sigma C\widetilde{T}^4 - G) \tag{9}$$

where G is the total irradiance.

2.4. Extinction modelling

Flame extinction is modelled using the default approach of FDS in LES mode which considers an enthalpy balance based on the concept of a critical flame temperature (CFT). The extinction criterion examines whether a reactant mixture within a computational cell will have enough energy to raise its temperature above a critical flame temperature to sustain combustion and it is expressed as [24]:

$$Z_F^0 h_F(\widetilde{T}) + \widetilde{\phi} Z_A^0 h_A(\widetilde{T}) + \widetilde{\phi} Z_P^0 h_P(\widetilde{T}) < Z_F h_F(T_{CFT}) + [Z_P - (1-\widetilde{\phi}) Z_P^0] h_P(T_{CFT}) \quad (10)$$

where Z_F^0, Z_A^0, Z_P^0 and Z_F, Z_A, Z_0 are the mass fractions of lumped species for fuel, air, and products in the mixed portion of the grid cell at the beginning and the end of the reaction step, respectively, $\widetilde{T}$ is the (filtered) initial cell temperature (before any reaction occurs), T_{CFT} is the critical flame temperature, while $h_F(\widetilde{T})$ and $h_P(\widetilde{T})$ are the sensible enthalpy of fuel and products, respectively. Note that $h_A(\widetilde{T})$ accounts for both the chemical and sensible enthalpy; thus, the left-hand-side of Eq. (10) includes the heat release due to combustion. The products include the products of combustion and diluents such as water vapour from droplet evaporation. A modified form of the equivalence ratio, $\widetilde{\phi}$, can be written as:

$$\widetilde{\phi} \equiv \left(1, \frac{s Z_F^0}{Z_A^0}\right) = \frac{Z_A^0 - Z_A}{Z_A^0} \quad (11)$$

where s is the mass stoichiometric coefficient for air.

Note that the T_{CFT} values used by the model have been measured experimentally (i.e., not derived theoretically considering adiabatic chemistry). As such, the right-hand-side of Eq. (10) implicitly accounts for any radiative losses. The same applies to the left-hand side of Eq. (10) since the resolved flame temperatures used in the model in each cell have been obtained considering radiative losses.

Based on the formulation of the model, any excess fuel within a cell acts as a diluent while any excess air and a proportional amount of products do not. To achieve this, a fraction of the total mass of the grid cell equal to $(1-\widetilde{\phi})(Z_A^0 + Z_P^0)$ has been removed from the calculation of the enthalpy. Note that the right-hand side of Eq. (10) contains no air because all excess air has been removed from consideration. In other words, for an infinitely fast reaction it is $Z_A - (1-\widetilde{\phi}) Z_A^0 \equiv 0$. In addition, there is no distinction between quenched and unquenched fuel in the model. If the inequality is true then reaction within a computational cell is inhibited for the current time step.

For the evaluation of the flame extinction criterion, a critical flame temperature, T_{CFT}, is needed. FDS uses by default a constant T_{CFT} value which is dependent on the fuel type and typically ranges between 1500–1800 K [33].

2.5. Re-ignition modelling

The flame extinction criterion discussed above is only evaluated if re-ignition in a cell can occur (i.e., if the initial temperature in the cell, $\widetilde{T}$, is above an ignition temperature):

$$\widetilde{T} \geq T_{ign} \quad (12)$$

where T_{ign} is set by default to the Auto-Ignition Temperature (AIT) of the fuel [33]. If Eq. (12) is not fulfilled, the combustion is automatically suppressed.

Note that the re-ignition sub-model cannot be applied everywhere in the computational domain without also suppressing the main combustion source. As such, a small exclusion zone surrounding the burner is typically defined. Ideally, this exclusion region should be as small as possible without negatively affecting the combustion efficiency of the fire. It should not be too big, either, so as to allow for the extinction criterion to be evaluated in a big portion of the flame where combustion takes place.

2.6. Dynamic extinction and re-ignition modelling approach

The new dynamic approach (named 'New model' from now on) is essentially an extension of the original flame extinction/re-ignition sub-models currently available in FDS (i.e., still relies on Eqs. (10) and (12)). However, the re-ignition temperatures, T_{ign}, required for re-ignition are estimated on the basis of counterflow simulations with oxidizers for different strain rates. Following [34], diluted fuel-air mixtures (i.e., 8% CH_4 in N_2), in the fuel stream, versus hot air at ambient oxygen concentration, in the oxidizer stream, at a pressure of 1 atm are considered. The temperatures of both the fuel and oxidizer were set to be the same. On the other hand, the determination of the critical flame temperatures, T_{CFT}, is made through well-stirred reactor simulations under different residence times and diluent types/concentrations. The simulations for both configurations have been performed with Cantera [35] using the FFCM-2 mechanism [36] which considers 96 species and 1054 reactions. A detailed description of the determination of T_{ign} and T_{CFT} used in the new dynamic model has been presented in [22], hence, only a brief summary of the resulting equations is reported here.

The variation of the re-ignition temperatures, T_{ign}, with CH_4 as fuel, follows a logarithmic function in the form:

$$T_{ign} = 135.84 \ln(S) + 411.52 \quad (13)$$

where S (1/s) is the strain rate and the T_{ign} values are bounded between 700–1250 K. In the simulations, the resolved strain rate magnitude in every cell is used for estimating T_{ign}.

The variation of the critical temperatures, T_{CFT}, with CH_4 as fuel, is fitted using power law lines in the form:

$$T_{CFT-N_2,CO_2} = 1522.1 \tau_{mix}^{-0.038} \quad (14)$$

$$T_{CFT-H_2O} = 1576.4 \tau_{mix}^{-0.027} \quad (15)$$

with N_2,CO_2 and H_2O as diluents, respectively. In the equations above, τ_{mix} (ms) is the mixing time obtained from the default reaction time scale model [28] available in FDS. The T_{CFT} values are bounded between 1200–1800 K, a range of values common for most hydrocarbon fuels [33].

Finally, the critical flame temperature in every cell is calculated using a mass-weighted average based on the different types of diluents as:

$$T_{CFT} = \sum_i Y_i' T_{CFT-i} \quad (16)$$

where i is the type of diluent (i.e., N_2, CO_2 or H_2O), Y_i' is the normalized mass fraction of diluent i and $T_{CFT,i}$ is the critical flame temperature for the type of diluent (i.e., T_{CFT-N_2,CO_2} or T_{CFT-H_2O}).

For completeness, the variation of T_{ign} and T_{CFT} is also presented graphically in Fig. 1. The values of the original approach of FDS (named 'Original model' from now on), using constant values for T_{ign} (i.e., 813 K for CH_4 [37]) and T_{CFT} (i.e., 1780 K for CH_4 [37]), are also reported.

It is worth noting that grid dependency can have some effect in the predictions of the new model (i.e., resulting combustion efficiency) if small fire sources (in terms of Q* values) are involved (which is not the case here). This has been previously demonstrated in [22] where the model was first developed and validated in open flame scenarios. It should be stressed that the model is meant for LES, hence a reasonable grid resolution of the fire plume is needed and required. The use of an exclusion zone, in combination with the considered grid size, can, in general, affect the resulting combustion efficiency and whether a stabilized fire plume above the burner will exist or not [22]. Nevertheless, regardless of how fine the grid resolution is, an exclusion zone (or prescribed pilot flames) is still needed to avoid suppressing the primary combustion source in the first couple of cells above the burner unless e.g., hot fuel would be injected into the domain.

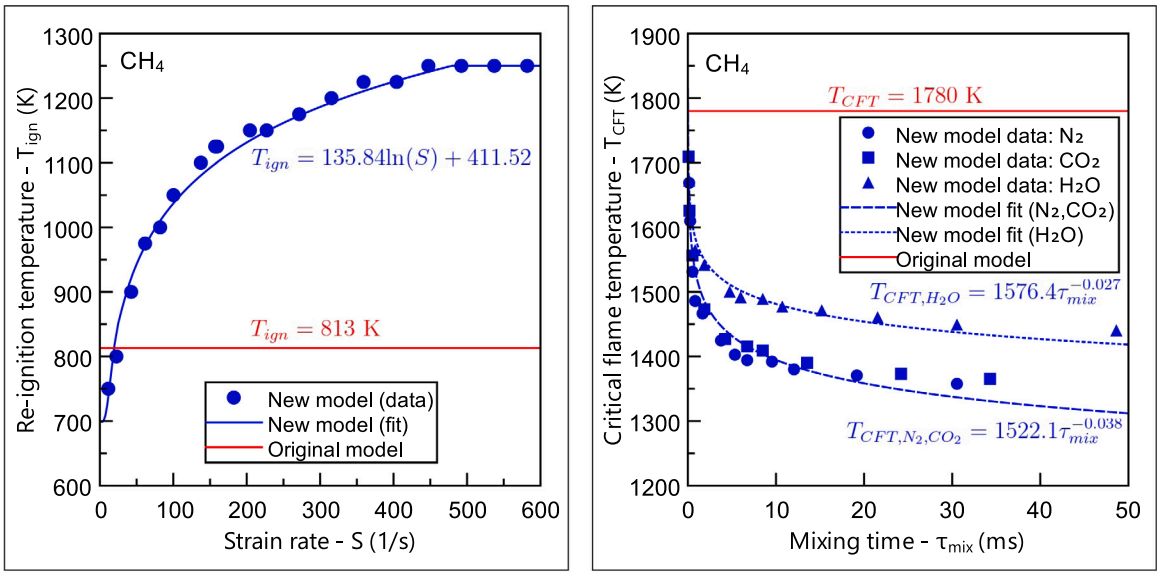

Fig. 1. Overview of the re-ignition temperatures, T_{ign}, and critical flame temperatures, T_{CFT}, used with both extinction models with CH_4 as fuel.

3. Experimental setup

The reduced-scale experiments performed by NIST [32], which involve a series of ventilation-controlled compartment fires, are used a validation test case for the simulations. The compartment is approximately 1.42 m long by 0.95 m wide by 0.98 m high and has a single ventilation opening (i.e., a door, centred on the smaller wall, with dimensions 0.48 m wide by 0.81 m high). The interior of the compartment consists of 0.0254 m thick Marinite I (i.e., $\rho = 737$ kg/m^3, $k = 0.12$ W/m/K, $c_p = 1.17$ kJ/kg/K) walls while in the exterior a 0.0016 m thick steel (i.e., $\rho = 7800$ kg/m^3, $k = 45$ W/m/K, $c_p = 0.77$ kJ/kg/K) frame is used. The scenarios involve a 0.13 m × 0.13 m (square) gravel-filled burner, positioned in the centre of the enclosure, which is 7 cm deep and its top surface is at 15 cm above the floor. The scenarios considered involve natural gas (CH_4) as fuel with a varying levels of HRR during the tests. Two experiments from the experimental campaign with varying total HRR between 75–410 kW are considered: test #1 with $\dot{Q}_{burner}$= 75, 190, 75 kW and test #3 with $\dot{Q}_{burner}$= 265, 410, 180, 115, 75 kW.

Thermocouple temperatures and species concentrations near the ceiling in the front and in the back of the compartment, as well as velocities at the ventilation opening (i.e., door), were reported among others. For a detailed discussion on the uncertainties involved in the different experimental data the reader is referred to [32]. An overview of the compartment geometry involved in the NIST reduced-scale experiments is presented in Fig. 2. For completeness, and to make the comparison between simulations and experiments easier, the location of the experimental probes that are considered in this work is reported in Table 1.

4. Numerical setup

An overview of the numerical setup used in the CFD simulations (e.g., domain, grid size and total number of cells, among others) is presented in Table 2. The required finest grid size is chosen a priori based on the D^* criterion by considering values of $D^*/\Delta \geq 15$, which have proven accurate enough for simulations of various fire scenarios with FDS in the past [29]. A sensitivity study considering grid sizes of 4 cm, 2 cm and 1 cm was also performed (i.e., only a selection of results are presented in Fig. 3 for brevity) and revealed a relatively grid-insensitive solution was reached with both models for a 2 cm grid size. The reader is referred to [22] for a more detailed evaluation of the performance of each extinction model with respect to grid size. The computational cost associated with the new model in the 2 cm grid size simulations was approximately 44 h and 63 h of wall clock time, for test #1 and test #3, respectively, using 24 cores.

The material and thickness of the compartment walls are the same as in the experiments (see Section 3). The numerical simulations account for conjugate heat transfer, by coupling the gas and solid phases, while 1D heat transfer is considered through the compartment walls. The ambient temperature and pressure are set to 20 °C and 101325 Pa, respectively. A value of 0.24 is assigned for the radiative fraction, χ_r, of CH_4 based on the experimental data reported in [38]. The default number of solid angles in FDS (i.e., 100) is employed in the simulations. For comparison to experimental data, a thermocouple (TC) model with the corresponding bead diameter (i.e., 1 mm), as used in the experiments, and the properties of Nickel (i.e., $\epsilon_{TC} = 0.85$, $\rho_{TC} = 8908$ kg/m^3 and $c_{p,\,TC} = 0.44$ kJ/(kg K)) [23] are considered. The thermocouple model considers the heating of a sphere, of known bead diameter, due to radiation (i.e., using the integrated radiative intensity) and convection (i.e., due to hot gasses). As such, the radiative term includes radiative contributions from both the fire itself but also from the (hot) walls.

An exclusion zone (i.e., a region inside which combustion is not suppressed) having dimensions of 0.16 m × 0.16 m × 0.06 m is considered in the study. The defined exclusion zone essentially considers one cell surrounding the burner in the transverse direction, a cell below the burner surface, and extends two cells above it in the vertical direction.

5. Results

A first qualitative overview of the numerical predictions with 'New model' and 'Original model' is depicted in Figs. 4 and 5 which present the instantaneous Heat Release Per Unit Volume (HRRPUV) (200 kW/m^3) at different times during the simulation for test #1 and test #3, respectively. The HRR of the burner at the same instances in time is also reported in the figures' captions. Combustion occurs mainly inside the compartment for test #1, apart from some minor burning just outside the ventilation opening at the time of the maximum HRR (i.e., 190 kW), indicating that mainly well-ventilated conditions are present during this scenario. On the other hand, combustion occurs clearly both inside and outside the enclosure in test #3 when the HRR of the burner is between

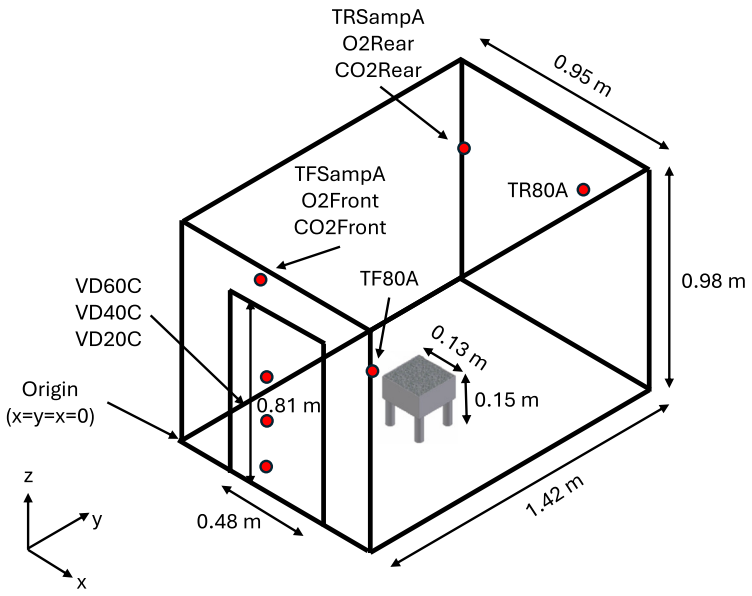

Fig. 2. Overview of the experimental geometry for the NIST reduced-scale enclosure scenario [32]. The approximate location of the measurement probes (see Table 1) used in the experiments is shown as red symbols.

Table 1
Location of measurement probes in the NIST reduced-scale experiments [32].

Probe description	Variable	Exp. data label	x (cm)	y (cm)	z (cm)
Aspirated thermocouple	Temperature	TRSampA	29	113	88
Aspirated thermocouple	Temperature	TFSampA	29	10	88
Aspirated thermocouple	Temperature	TR80A	75	122	80
Aspirated thermocouple	Temperature	TF80A	75	20	80
Gas sample rear	O_2	O2Rear	29	113	88
Gas sample front	O_2	O2Front	29	10	88
Gas sample rear	CO_2	CO2Rear	29	113	88
Gas sample front	CO_2	CO2Front	29	10	88
Bi-directional velocity probe	Velocity	VD60C	48	−5	60
Bi-directional velocity probe	Velocity	VD40C	48	−5	40
Bi-directional velocity probe	Velocity	VD20C	48	−5	20

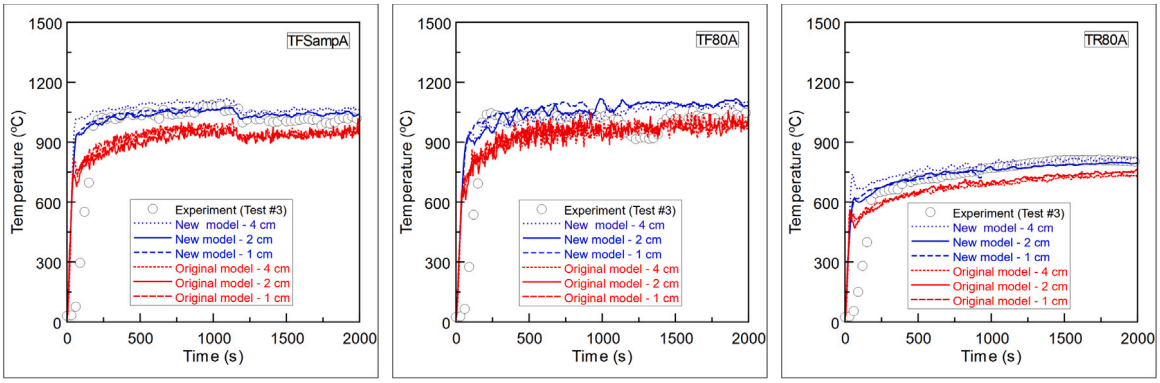

Fig. 3. Predicted thermocouple temperatures as a function of grid size at selected locations with 'New model' and 'Original model' in test #3.

265–410 kW, suggesting the presence of under-ventilated conditions inside the compartment during these times. As the HRR of the burner decreases (e.g., 180 kW), there is a transition to more well-ventilated conditions and combustion then occurs only inside the compartment with both models. Overall, no significant differences in the (overall) combustion region are observed between the results obtained with both models, for both tests.

To complement the qualitative analysis, an overview of the instantaneous temperatures with 'New model' and 'Original model' is presented in Figs. 6 and 7 at different times during the simulation for test #1 and test #3, respectively. Some observable differences between the models are evident, namely that higher temperatures are predicted with 'New model' inside the compartment most of the time. This aspect would suggest higher mixture reactivity inside the enclosure with 'New model' compared to 'Original model' as a result of different T_{ign} and T_{CFT} values used by each model. A more detailed analysis of this aspect is presented later in the paper.

An overview of the predicted total HRR, as well as of the HRR released outside of the enclosure, with the two models is presented in Fig. 8. The simulation results, in most cases, follow closely the

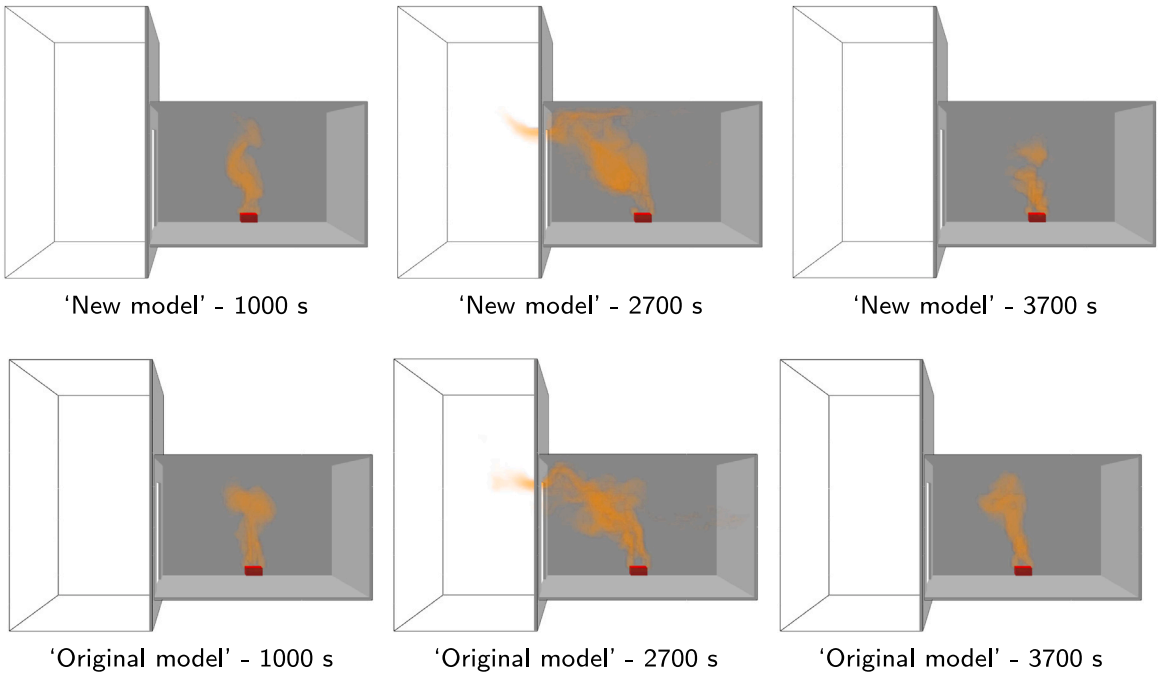

Fig. 4. Predicted HRRPUV (200 kW/m^3) with 'New model' (top row) and 'Original model' (bottom row) at 1000 s ($\dot{Q}_{burner}$ = 75 kW), 2700 s ($\dot{Q}_{burner}$ = 190 kW) and 3700 s ($\dot{Q}_{burner}$ = 75 kW) in test #1.

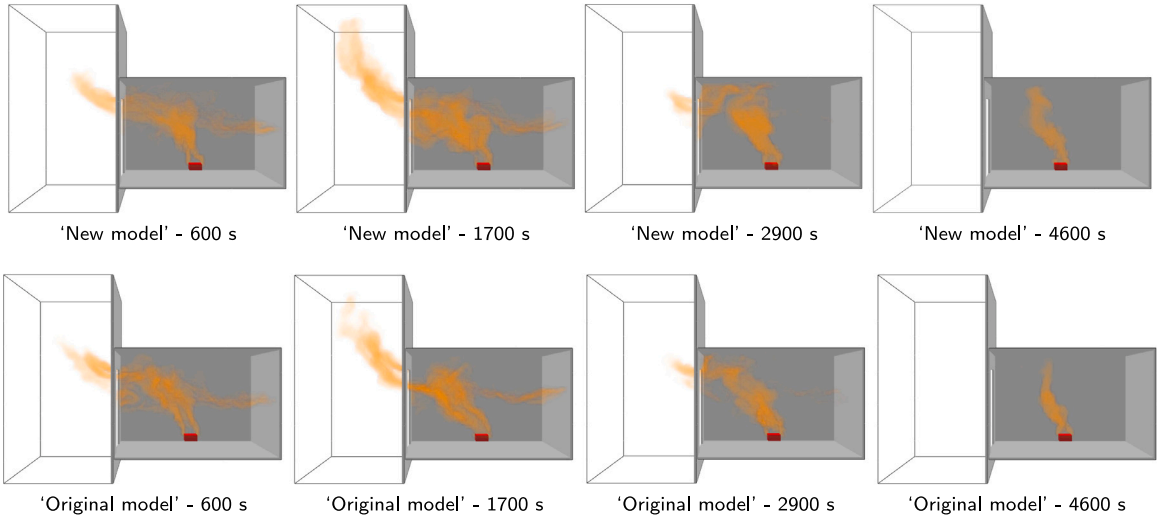

Fig. 5. Predicted HRRPUV (200 kW/m^3) with 'New model' (top row) and 'Original model' (bottom row) at 600 s ($\dot{Q}_{burner}$ = 265 kW), 1700 s ($\dot{Q}_{burner}$ = 410 kW), 2900 s ($\dot{Q}_{burner}$ = 180 kW) and 4600 s ($\dot{Q}_{burner}$ = 75 kW) in test #3.

experimental data, which is not surprising given the fact that the HRR issued from the burner was prescribed in the simulations. A slight under-prediction of the predicted HRR in the simulations is observed when $\dot{Q}_{burner}$ = 410 kW for both models, suggesting that small quantities of fuel (i.e., CH_4) might escape the computational domain unburned. This could be solved by making the domain outside the compartment even bigger but, to limit the required computing time, this was not deemed essential. Overall, the predictions with both 'New model' and 'Original model' are, both qualitatively and quantitatively, comparable. However, the results do indicate that slightly more fuel is burning outside the compartment with 'Original model' during both tests #1 and #3 when under-ventilated conditions start to develop (see the HRR 'Out' lines with both models in Fig. 8). This is in line with the higher T_{CFT} values used with this model (also previously reported in [22]).

Considering that hydrostatic pressure differences govern the gas flow at a compartment opening, and by considering Bernoulli's equation, the maximum heat release rate inside a compartment in under-ventilated fire scenarios, $\dot{Q}_{in}^{max}$ (kW), is often estimated as [39]:

$$\dot{Q}_{in}^{max} = Y_{O_{2,air}} \Delta H_{c,O_2} \underbrace{C A \sqrt{H}}_{\dot{m}_{air,in}} \approx 1500 A \sqrt{H} \tag{17}$$

where $Y_{O_{2,air}}$ is the oxygen mass fraction in ambient air (i.e., 0.23), $\Delta H_{c,O_2}$ the heat of combustion per mass of oxygen consumed (i.e., 13.1 MJ/kg), C is a flow coefficient (i.e., 0.5 kg/(s m$^{5/2}$) [40]) and $A\sqrt{H}$ (m$^{5/2}$) is the ventilation factor (where A and H is the surface area and height of the ventilation opening, respectively). Essentially $\dot{m}_{air,in}$ (kg/s) is the mass flow rate of incoming air inside the compartment from the ventilation opening and 1500 kJ/(s m$^{5/2}$) is a

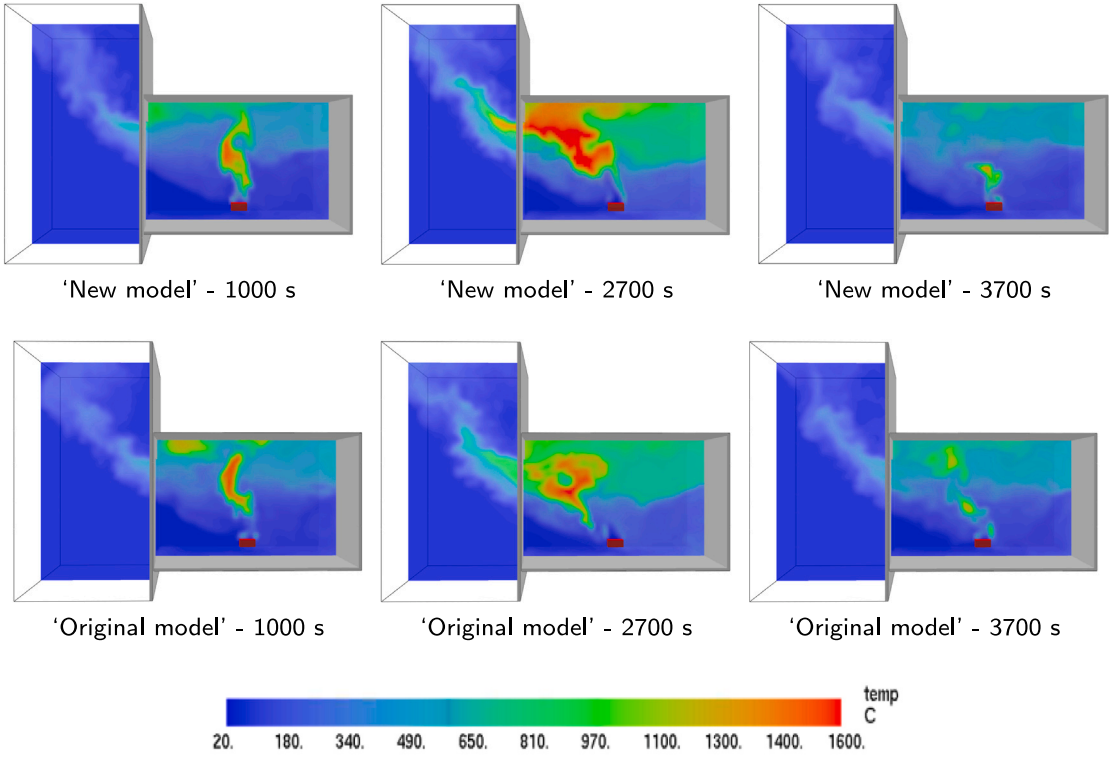

Fig. 6. Predicted instantaneous temperature with 'New model' (top row) and 'Original model' (bottom row) at 1000 s ($\dot{Q}_{burner}$ = 75 kW), 2700 s ($\dot{Q}_{burner}$ = 190 kW) and 3700 s ($\dot{Q}_{burner}$ = 75 kW) in test #1.

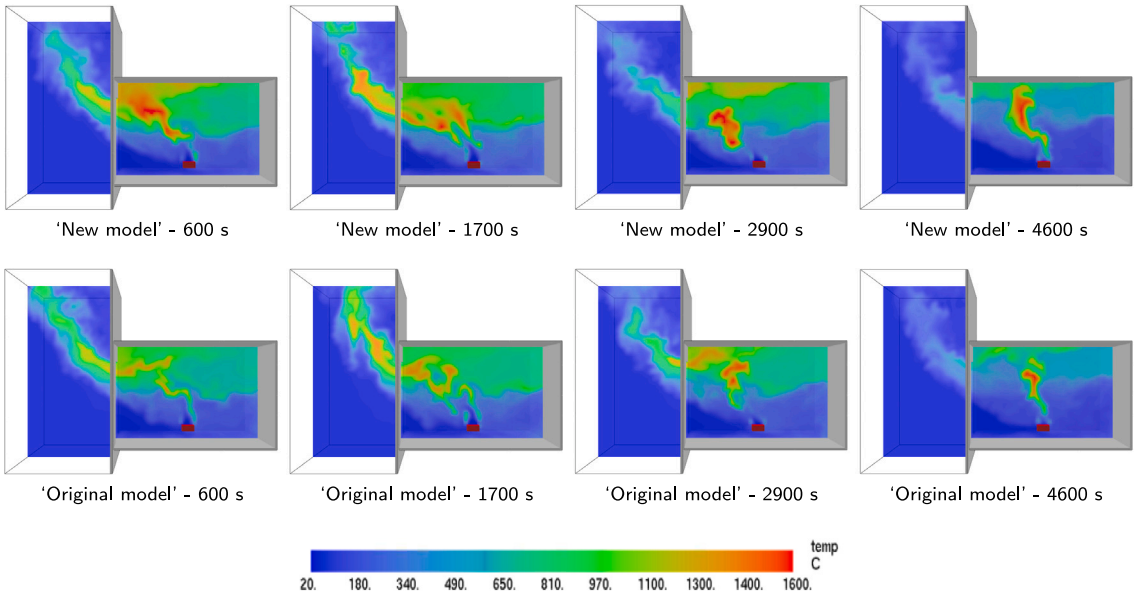

Fig. 7. Predicted instantaneous temperatures with 'New model' (top row) and 'Original model' (bottom row) at 600 s ($\dot{Q}_{burner}$ = 265 kW), 1700 s ($\dot{Q}_{burner}$ = 410 kW), 2900 s ($\dot{Q}_{burner}$ = 180 kW) and 4600 s ($\dot{Q}_{burner}$ = 75 kW) in test #3.

constant representing the thermal energy potential of the air entering the compartment.

Note that there are three approximations in Eq. (17): $\dot{m}_{air,in}^{max}$ is approximated as 0.5 $A\sqrt{H}$; there are uniform conditions (i.e., temperature, mixing) inside the compartment (which is often not the case unless the enclosure is small in size) and it is assumed that all of the oxygen entering the enclosure would be consumed during the combustion which is unlikely (e.g., it will strongly depend on the mixing between fuel and oxidizer, which is in turn dependent on the opening, the type of fuel, size and location of burner among other factors).

As such, much lower values of this constant (i.e., compared to the theoretical maximum value of 1500) have been reported in the literature for various compartment fire scenarios in the past (e.g., 850 kJ/(s m$^{5/2}$) [15], 900 kJ/(s m$^{5/2}$) [16], 1040–1290 kJ/(s m$^{5/2}$) [41] and 1131 kJ/(s m$^{5/2}$) [42] among others). In the current work (i.e., when $\dot{Q}_{burner}$ = 410 kW during test #3 with $A\sqrt{H} \approx 0.343$ m$^{5/2}$),

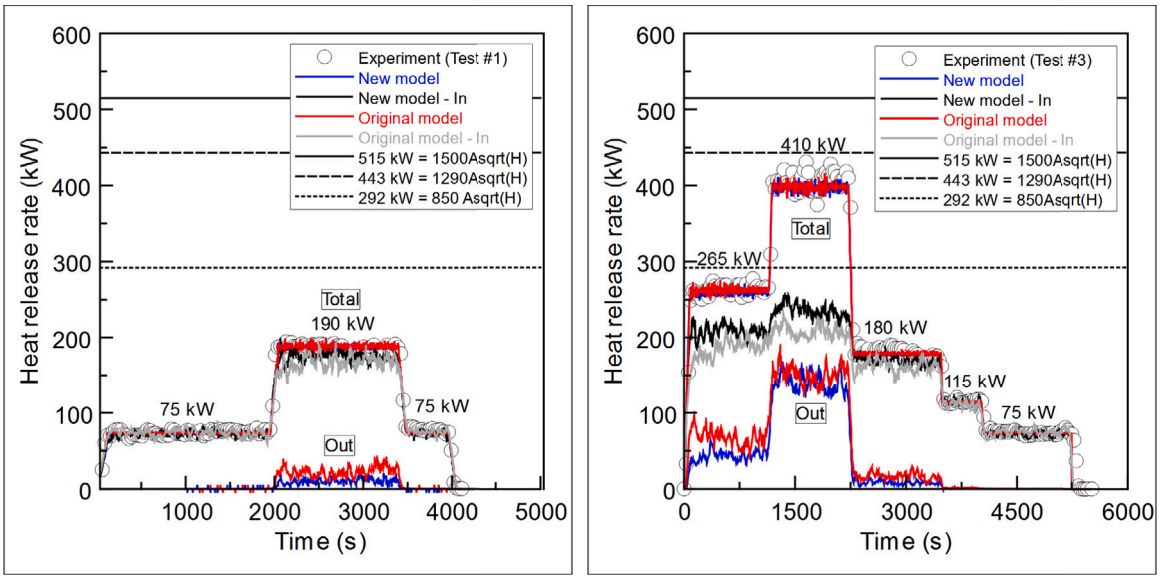

Fig. 8. Predicted HRR (total and outside the enclosure) with 'New model' and 'Original model' in (a) test #1 and (b) test #3.

Table 2
Overview of the setup used in the numerical simulations.

Fuel	CH_4
Burner	0.12 m × 0.12 m[a]
HRR ($\dot{Q}_{burner}$)	75–190 kW (test #1), 75–410 kW (test #3)
Domain (compartment) Domain (outside)	1.42 m × 0.96 m × 0.98 m 0.9 m × 1.2 m × 1.8 m
Grid size (Δ)	2 cm
D^*[b]	0.34–0.67 m
ResoIution index[c]	17–34
Number of cells (gas phase)	0.41 million

[a] Adjusted from the actual size of 0.13 m × 0.13 m to fit the chosen grid size, Δ, in the simulations.

[b] Characteristic fire diameter [24]: $D^* = \left(\frac{\dot{Q}_{burner}}{\rho_\infty c_p T_\infty \sqrt{g}}\right)^{2/5}$ where $\dot{Q}_{burner}$ (kW) is the heat release rate issued from the burner, ρ_∞ (kg/m^3), c_p (kJ/(kg K)), T_∞ (K) are the density, specific heat and temperature of the ambient air, respectively, while g (m/s^2) is the gravitational acceleration.

[c] Resolution index (RI) defined as D^*/Δ [24]. The reported range involves the same grid size and a variable HRR.

it is $\dot{m}_{air,in} = 0.305A\sqrt{H}$ and $\dot{Q}_{in} = 686A\sqrt{H}$ for 'New model', while $\dot{m}_{air,in} = 0.312A\sqrt{H}$ and $\dot{Q}_{in} = 606A\sqrt{H}$ for 'Original model'. Note that, despite the higher mass flow rate of incoming air, $\dot{m}_{air,in}$, the HRR inside the enclosure, $\dot{Q}_{in}$, is lower for the 'Original model'. The difference (i.e., 606/0.312 versus 686/0.305) is about 16%. Note that for the calculations above, the door dimensions (i.e., $H = 0.8$ m and $A = 0.48$ m × 0.8 m) used in the simulations have been considered.

Based on the available experimental results, it can be verified that the combustion efficiency was close to 1 for both tests #1 and #3. Using Eq. (17), a theoretical maximum HRR of approximately 515 kW is obtained. On the other hand, the use of a reduced constant (i.e., 850–1290 kJ/(s m$^{5/2}$)), as discussed above, results in a range of HRR values between approximately 292–443 kW. As such, the initial variation of the HRR during test #3 (i.e., 265–410 kW) is close to this range of HRR values, suggesting the potential presence of under-ventilated conditions during this test. On the other hand, the HRR values involved during test #1 are significantly lower. This is also in line with the burning occurring outside of the compartment previously as seen qualitatively in Fig. 5 and quantitatively in Fig. 8.

One way to quantify the ventilation conditions in the compartment scenarios at hand, is the use of the global equivalence ratio [39,43]:

$$\phi = \frac{s\dot{m}_f}{\dot{m}_{O_2}} \tag{18}$$

where s is the stoichiometric fuel to oxygen ratio (i.e., $s \approx 4$ for CH_4), $\dot{m}_f$ is the fuel mass flow rate at the burner, and $\dot{m}_{O_2}$ is the oxygen mass flow rate entering the compartment from the ventilation opening. Based on this definition, the distinction is often made between over-ventilated compartment fires (if $\phi < 1$) and under-ventilated compartment fires (if $\phi > 1$) [39,43].

Based on Fig. 9, values of $\phi > 1$ are only obtained when $\dot{Q}_{burner} = 410$ kW during test #3, indicating the presence of under-ventilated conditions during that period of time, while for all other scenarios it is $\phi < 1$. The fact that $\phi < 1$ when $\dot{Q}_{burner} = 265$ kW during test #3 (when external burning is predicted with both models) does suggest that part of the incoming air does not participate in the combustion. In other words, the concept of the global equivalence ratio using a critical value for ϕ of 1 does not accurately distinguish when under- and over-ventilated conditions develop inside a compartment (i.e., the critical value of ϕ becomes significantly less than 1 as reported in, e.g., [44,45]). While the use of ϕ is representative of the bulk conditions present inside a compartment, the local conditions near the fire source are particularly important with respect to potential flame extinction and external burning occurring in a compartment fire scenario.

The predicted T_{ign} and T_{CFT} values at two different locations above the burner (i.e., in the flame/intermittent region ($z = 0.3$ m) and below the ceiling ($z = 0.9$ m)) are presented in Fig. 10 for both tests. In general, mostly higher T_{ign} but lower T_{CFT} values are obtained with 'New model' compared to 'Original model'. In other words, re-ignition is more difficult with 'New model' to occur as opposed to 'Original model'. However, once re-ignited then extinction is easier for 'Original model' to occur as opposed to 'New model'. The reported range of T_{ign} and T_{CFT} values at these two specific locations is approximately 750–1050 K and 1300–1400 K, respectively.

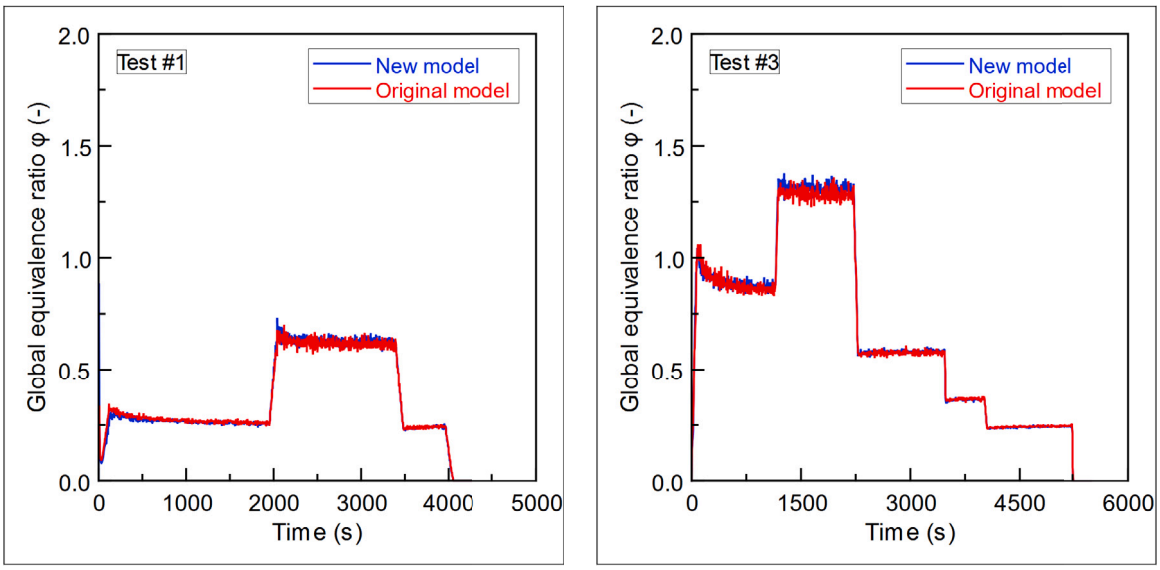

Fig. 9. Predicted global equivalence ratio, ϕ, with 'New model' and 'Original model' in (a) test #1 and (b) test #3.

A comparison of the predicted thermocouple temperatures and species concentrations with 'Original model' and 'New model' at selected locations (see Table 1) for test #1 and test #3 is presented in Figs. 11–12. Overall, both models exhibit similar trends which are, in most cases, in line with what was recorded experimentally. Some differences between the two models are mainly observed for the highest range of HRRs involved in both tests (i.e., when $\dot{Q}_{burner} = 190$ kW for test #1 and when $\dot{Q}_{burner} = 265 - 410$ kW for test #3). It is not straightforward to definitively say which of the two models performs best by only looking at the temperature results. Nevertheless, when examined in combination with the chemical species results (i.e., particularly the predicted O_2 and CO_2 concentrations) an interesting pattern emerges. During the highest HRRs for both test #1 and test #3, the O_2 concentrations with 'New model' tend to zero (which is not the case with 'Original model'), in line with the experimental measurements, and more CO_2 is produced. Similar findings with respect to the O_2 concentrations with 'Original model' have also been reported for the same test case in [29]. This is in line with the fact that relatively more burning occurs inside the compartment and higher temperatures are obtained with 'New model' compared to 'Original model'. This is not the case with 'Original model', where some O_2 remains at the examined locations, lower temperatures and less CO_2, compared to 'New model', is produced. Similar findings were also reported in [22] related to the application of both models in benchmark burner scenarios involving flame extinction (i.e., UMD line burner and FM burner cases).

There is naturally a combined effect from both the re-ignition and critical flame temperatures in the overall mixture reactivity with the new model inside the compartment. For example, higher flame temperatures suggest that the lower critical flame temperatures must have an important contribution. On the other hand, the higher O_2 concentrations predicted with the new model imply less mixture reactivity due to higher re-ignition temperatures. The relative contribution of each of these two aspects is also dependent on the location of interest inside the compartment and whether unburned fuel is present or not.

It is worth noting that no sensitivity study using the original FDS model with adjusted but constant T_{CFT} and T_{ign} values was conducted as it was not part of the main objectives of this work. It is probable that fine-tuning these constants could improve the original model predictions in these compartment fire scenarios, but this is not considered of significant added scientific value to the present study.

Finally, it should be noted that the predicted CO_2 concentrations in the simulations will inevitably also be dependent on any sub-models for CO production. Accurate prediction of CO in ventilation-controlled compartment fire scenarios is challenging and still an active field of research in the fire community. Given the fact that relatively small amounts of CO were produced during the experiments considered and that CO is not directly involved in the newly developed model, it was decided to avoid the added modelling uncertainties associated with trying to predict CO as well during the simulations. The effect of CO production will be considered in future modelling of compartment scenarios, though.

The predicted velocities at the level of the ventilation opening (i.e., door), presented in Fig. 13, are comparable for both models and are, in most cases, comparable to the experimental data. This implies that the extinction model, even though it might locally affect the predicted flame temperatures, does not have any major influence on the resulting flow field. With comparable amounts of fresh air coming inside the compartment, it is then the differences in the extinction (through T_{CFT}) and re-ignition (through T_{ign}) modelling that give rise to differences in the flame temperatures and species compositions between the two models.

6. Conclusions

Large eddy simulations of ventilation-limited compartment fire scenarios with natural gas (CH_4) as fuel were performed with FDS (version 6.9.1) in LES mode using a new dynamic flame extinction and re-ignition model. The re-ignition temperatures, used to determine potential re-ignition of the fuel, were estimated from counterflow simulations with hot oxidizers at different strain rates. The estimation of the critical flame temperatures, used to determine potential flame extinction, was made through well-stirred reactor simulations under different residence times and diluent types/concentrations. Both configurations were simulated using Cantera. A comparison against experimental data and with the original extinction and re-ignition models of FDS, employing constant re-ignition and flame extinction temperatures for the same fuel, was also performed.

In general, more burning occurs inside the compartment with the new model, compared to the original model of FDS, and there is a

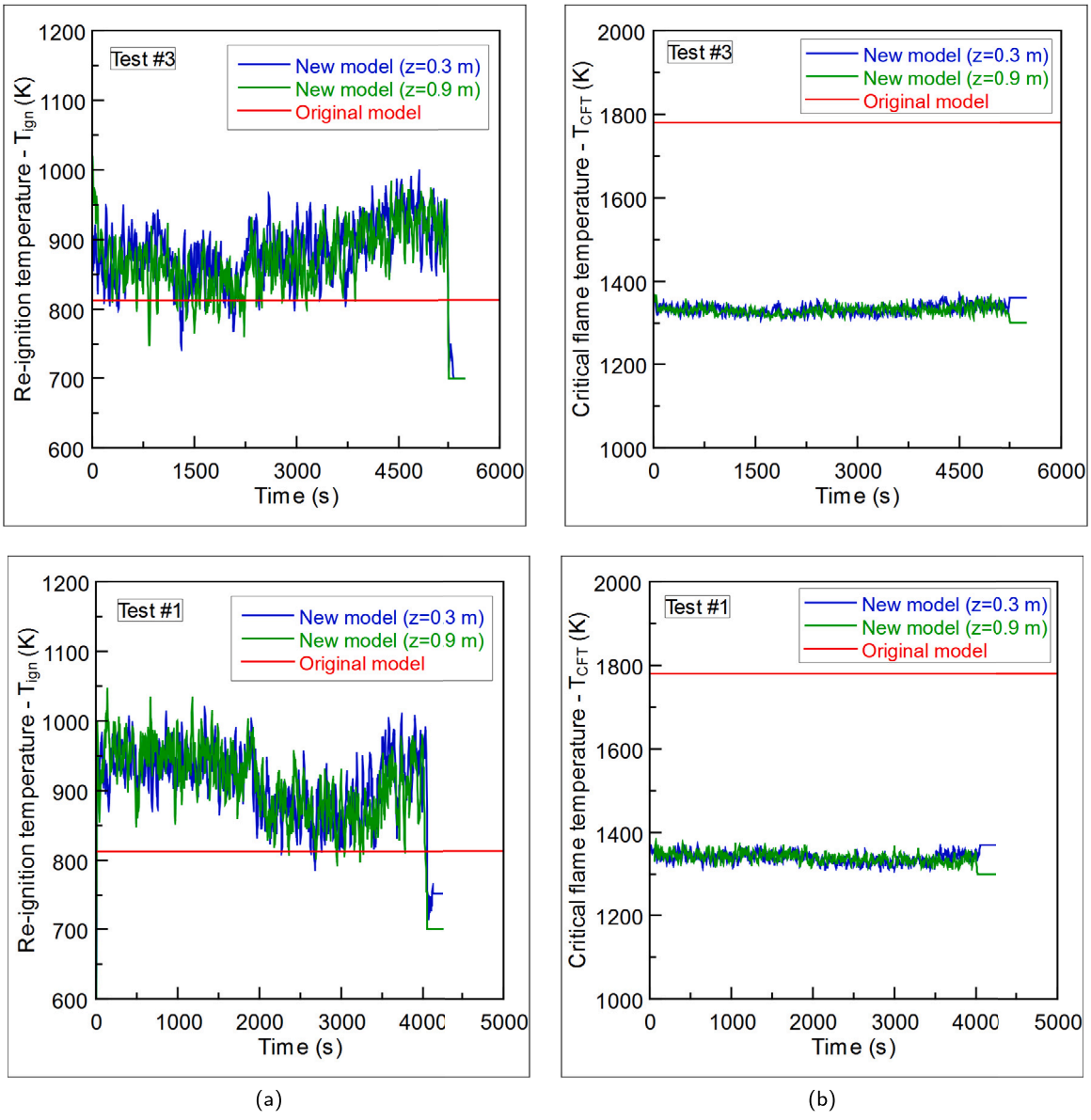

Fig. 10. Predicted (a) T_{ign} and (b) T_{CFT} values at different heights above the burner with 'New model' and 'Original model' in test #1 (bottom row) and test #3 (top row).

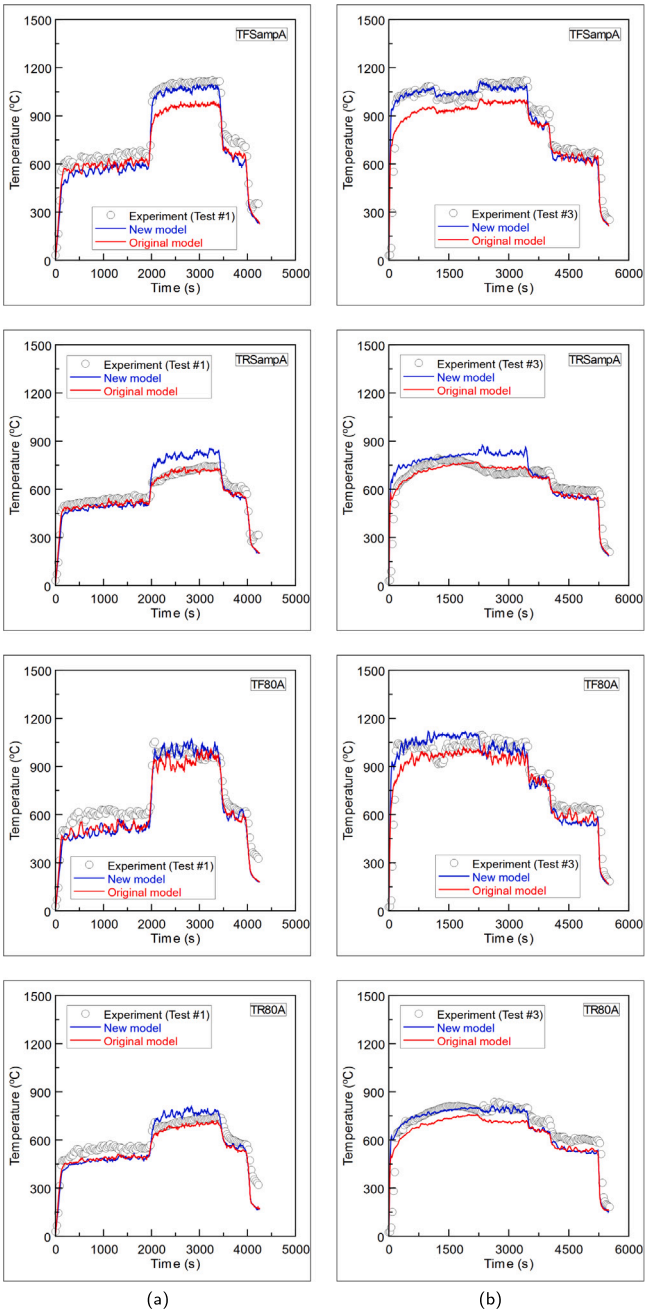

Fig. 11. Predicted thermocouple temperatures at the various locations with 'New model' and 'Original model' in (a) test #1 and (b) test #3.

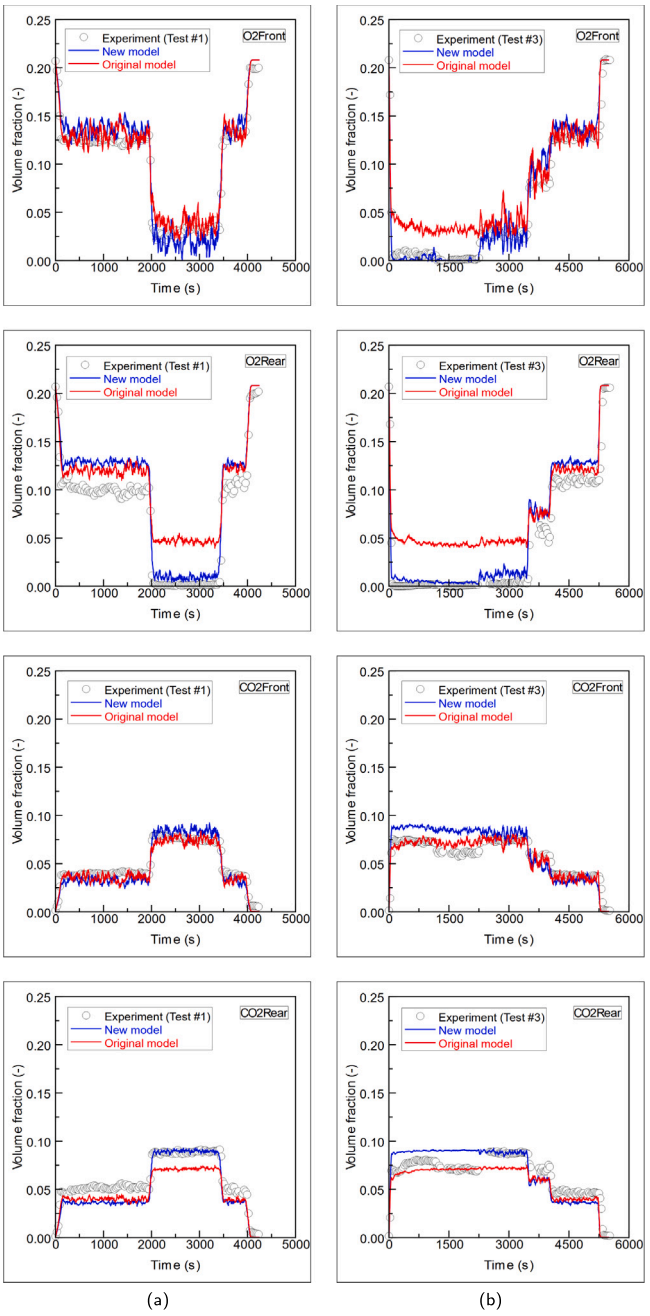

Fig. 12. Predicted O_2 vol. fraction and CO_2 vol. fraction at the various locations with 'New model' and 'Original model' in (a) test #1 and (b) test #3.

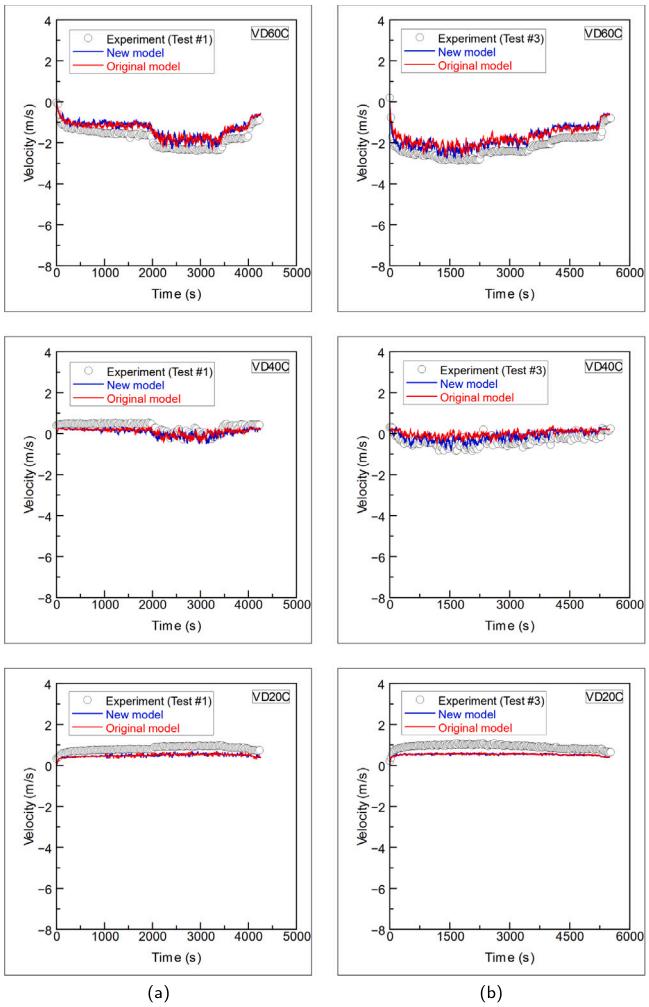

Fig. 13. Predicted velocities at different locations at the door with 'New model' and 'Original model' in (a) test #1 and (b) test #3.

better prediction of the flame temperatures and the O_2 concentrations at the locations examined. The predicted re-ignition temperatures with the model were often higher than the default values used by FDS (i.e., 750–1050 K versus 813 K for CH_4) while the predicted critical flame temperatures were significantly lower than the default values used by FDS (i.e., 1300–1400 K versus 1780 K for CH_4). In addition, the predicted HRR inside the compartment was significantly lower (i.e., $686A\sqrt{H}$) than the often cited theoretical maximum value (i.e., $1500A\sqrt{H}$) because not all of the incoming air in the compartment participated in the combustion.

Overall, the application of the new dynamic extinction and re-ignition models illustrated that improvements can be made in the FDS predictions of ventilation-limited compartment fire scenarios by considering the local properties of the flow. Further model validation considering additional compartment scenarios and fuels will be made in the future.

CRediT authorship contribution statement

Georgios Maragkos: Writing – original draft, Visualization, Validation, Software, Methodology, Investigation, Formal analysis, Data curation, Conceptualization. **Jason Floyd:** Writing – review & editing, Software. **Andrea Lucherini:** Writing – review & editing, Funding acquisition. **Alexander Snegirev:** Writing – review & editing. **Elijah Igweh:** Writing – review & editing. **Bart Merci:** Writing – review & editing, Supervision, Project administration, Funding acquisition.

Declaration of competing interest

The authors declare the following financial interests/personal relationships which may be considered as potential competing interests: Bart Merci, Andrea Lucherini reports financial support was provided by UL Fire Safety Research Institute. Andrea Lucherini, Elijah Igweh reports financial support was provided by European Union. Bart Merci, Alexander Snegirev reports financial support was provided by European Research Council. If there are other authors, they declare that they have no known competing financial interests or personal relationships that could have appeared to influence the work reported in this paper.

Acknowledgements

This research is funded by the UL Research Institutes' Fire Safety Research Institute through project 1492830. Andrea Lucherini and Elijah Igweh would like to gratefully acknowledge the financial support for the FRISSBE project within the European Union's Horizon 2020 research and innovation programme (GA 952395). This work is also supported by ERC grant FireSpace, 101224129, GAP-101224129.

Data availability

Data will be made available on request.

References

[1] Kawagoe K. Fire Behavior in Rooms. Report 27, Tokyo, Japan: Building Research Institute, Ministry of Construction; 1958.
[2] Thomas PH, Heselden AJM. Fully developed fires in single compartments. In: Fire Research Note 923. CIB Report No 20, Borehamwood, England, UK: Fire Research Station; 1972.
[3] Torero JL, Majdalani AH, Abecassis-Empis C, Cowlard A. Revisiting the compartment fire. Fire Saf Sci 2014;11:28–45.
[4] Novozhilov V. Computational fluid dynamics modeling of compartment fires. Prog Energy Combust Sci 2001;27:611–66.
[5] Trouvé A, Wang Y. Large eddy simulation of compartment fires. Int J Comput Fluid Dyn 2010;24:449–66.
[6] Beji T, Hidalgo JP, Fateh T, Floyd J, H. Pr´ etrel A Hamins. Compartment fires: Challenges for fire modeling as a tool for a safe design (IAFSS workshop,april 2021). Fire Saf J 2024;144:104109.
[7] Floyd JE, McGrattan KB, Hostikka S, Baum HR. CFD fire simulation using mixture fraction combustion and finite volume radiative heat transfer. J Fire Prot Eng 2003;13:11–36.
[8] Suard S, Lapuerta C, Babik F, Rigollet L. Verification and validation of a CFD model for simulations of large-scale compartment fires. Nucl Eng Des 2011;241:3645–57.
[9] Wahlqvist J, van Hees P. Validation of FDS for large-scale well-confined mechanically ventilated fire scenarios with emphasis on predicting ventilation system behavior. Fire Saf J 2013;62:102–14.
[10] Lee J, Kim B, Lee S, Shin WG. Validation of the fire dynamics simulator (FDS) model for fire scenarios with two liquid pool fires in multiple compartments. Fire Saf J 2023;141:103892.
[11] Suard S, Lapuerta C, Kaiss A, Porterie B. Sensitivity analysis of a fire field model in the case of a large-scale compartment fire scenario. Numer Heat Transf Part A Appl 2013;63:879–905.
[12] Vilfayeau S, Ren N, Wang Y, Trouvé A. Numerical simulation of under-ventilated liquid-fueled compartment fires with flame extinction and thermally-driven fuel evaporation. Proc Combust Inst 2015;35:2563–71.
[13] Beji T, Merci B. Blind simulation of periodic pressure and burning rate instabilities in the event of a pool fire in a confined and mechanically ventilated compartment. Combust Sci Technol 2016;188:504–15.
[14] Ukairo O, Dembele S, Heidari A, Pretrel H, Wen J. Investigation of fires in a mechanically ventilated compartment using the CFD code firefoam. Nucl Eng Des 2021;384:111515.
[15] Lafdal B, Djebbar R, Boulet P, Mehaddi R, Koutaiba E, Beji T, Torero JL. Numerical study of the combustion regimes in naturally-vented compartment fires. Fire Saf J 2022;131:103604.
[16] Mehaddi R, Lafdal B, Boulet P. Numerical and experimental investigation of shaft-like compartment fires. Fire Saf J 2025;158:104521.
[17] Lucherini A, Torero JL. Defining the fire decay and the cooling phase of post-flashover compartment fires. Fire Saf J 2023;141:103965.
[18] Merci B, Li J, Maragkos G. On the importance of the heat release rate in numerical simulations of fires in mechanically ventilated air-tight enclosures. Proc Combust Inst 2023;39:3647–72.
[19] Fire Dynamics Simulator (FDS). 2026, https://pages.nist.gov/fds-smv/. (accessed on 28 April 2026).
[20] Lafdal RMehaddi B, Boulet P. Numerical and experimental investigation of compartment fires. J Phys : Conf Ser 2024;2885:012036.
[21] Burdun A, Boulet P, Koutaiba E, Lafdal B, Mehaddi R, A. Trouv´ e CFD Modeling in Compartment Fires, Phys J. Conf. Ser 2025;3121:012024.
[22] Maragkos G, Floyd J, Lucherini A, Snegirev A, Igweh E, Merci B. Development and application of a dynamic flame extinction and re-ignition model in FDS. 2026,
[23] McGrattan K, Hostikka S, Floyd J, McDermott R, Vanella M, Muelelr E, Paul C. Fire dynamics simulator user's guide,national bureau of standards. In: NIST special publication 1019. Sixth ed.. 2025.
[24] McGrattan K, Hostikka S, Floyd J, McDermott R, Vanella M, Mueller E, Paul C. Fire Dynamics Simulator Technical Reference Guide Volume 1: Mathematical Model. Sixth ed.. National Institute of Standards and Technology, NIST Special Publication; 2025, p. 1–1018.
[25] Deardorff JW. Stratocumulus-capped mixed layers derived from a three-dimensional model. Bound -Layer Meteorol 1980;18:495–527.
[26] Pope SB. Turbulent flows. first ed.. Cambridge: Cambridge University Press; 2000.
[27] Magnussen BF, Hjertager BH. On mathematical modeling of turbulent combustion with special emphasis on soot formation and combustion. Symp (Int.) Combust 1977;16:719–29.
[28] McDermott R, McGrattan K, Floyd J. A simple reaction time scale for under-resolved fire dynamics. Fire Saf Sci 2011;10:809–20.
[29] McGrattan K, Hostikka S, Floyd J, McDermott R, Vanella M, Mueller E, Paul C. Fire Dynamics Simulator Technical Reference Guide Volume 3: Validation. Sixth ed.. National Institute of Standards and Technology, NIST Special Publication; 2025, p. 3–1018.
[30] Heskestad G. Engineering relations for fire plumes. Fire Saf J 1984;7:25–32.
[31] Grosshandler W. RadCal: A Narrow Band Model for Radiation Calculations in a Combustion Environment. National Institute of Standards and Technology; 1993, NIST Technical Note 1402.
[32] Bundy M, Hamins A, Johnsson E, Kim S, Ko G, Lenhert D. Measurements of Heat and Combustion Products in Reduced-Scale Ventilation-Limited Compartment Fires. Gaithersburg, MD: National Institute of Standards and Technology; 2007, NIST Technical Note 1483.
[33] Beyler C. SFPE handbook of fire protection engineering, chapter flammability limits of premixed and diffusion flames. fifth ed.. New York: Springer; 2016.
[34] Fotache CG, Kreutz TG, Law CK. Ignition of hydrogen-enriched methane by heated air. Combust Flame 1997;110:429–40.
[35] Goodwin DG, Moffat HK, Schoegl I, Speth RL, Weber BW. Cantera: An object-oriented software toolkit for chemical kinetics, thermodynamics, and transport processes. 2023, http://dx.doi.org/10.5281/zenodo.8137090, Version 3.0.0.
[36] Foundational fuel chemistry model version 2.0. 2026, https://web.stanford.edu/group/haiwanglab/FFCM2/. (accessed on 28 April 2026).
[37] SFPE Handbook of Fire Protection Engineering. Springer; 2016, p. 3.111.
[38] White JP, Link ED, A.C. Trouv´ e PB Sunderland, Marshall AW, Sheffel JA, Corn ML, Colket MB, Chaos M, Yu H-Z. Radiative emissions measurements from a buoyant, turbulent line flame under oxidizer-dilution quenching conditions. Fire Saf J 2015;76:74–84.
[39] Karlsson B, Quintiere JG. Enclosure fire dynamics. CRC Press; 2000.
[40] Babrauskas V. Estimating room flashover potential. Fire Technol 1980;16:94–103, 1980.
[41] Wang Z, Zhang T, Huang X. Numerical modeling of compartment fires: Ventilation characteristics and limitation of kawagoe's law. Fire Technol 2024;60:1245–68.
[42] Zhao G, Beji T, Merci B. Application of FDS to under-ventilated enclosure fires with external flaming. Fire Technol 2016;52:2117–42.
[43] Drysdale D. An introduction to fire dynamics. third ed.. New York: John Wiley & Sons; 2011.
[44] H. Prétrel JAt Thabari, Maragkos G, Moorthamers Y, Snegirev AY, Merci B. New insights into burning regimes in a closed mechanically ventilated compartment through experimental and theoretical analysis. Fire Saf J 2026;160:104602.
[45] H. Prétrel JAt Thabari, Maragkos G, Moorthamers Y, Snegirev A, Merci B. The importance of the GER definition in the analysis of combustion regimes in a closed mechanically ventilated compartment. J Phys: Conf Ser 3 2025;121:012015.